

Azimuthal anisotropy of direct photons in Au+Au collisions at $\sqrt{s_{NN}} = 200$ GeV

N.J. Abdulameer,^{15,22} U. Acharya,¹⁹ A. Adare,¹² C. Aidala,⁴² N.N. Ajitanand,^{60,*} Y. Akiba,^{55,56,†} M. Alfred,²¹ S. Antsupov,⁵⁸ N. Apadula,^{27,61} H. Asano,^{34,55} B. Azmoun,⁷ V. Babintsev,²³ M. Bai,⁶ N.S. Bandara,⁴⁰ B. Bannier,⁶¹ E. Bannikov,⁵⁸ K.N. Barish,⁸ S. Bathe,^{5,56} A. Bazilevsky,⁷ M. Beaumier,⁸ S. Beckman,¹² R. Belmont,^{12,49} A. Berdnikov,⁵⁸ Y. Berdnikov,⁵⁸ L. Bichon,⁶⁶ B. Blankenship,⁶⁶ D.S. Blau,^{33,46} J.S. Bok,⁴⁸ V. Borisov,⁵⁸ K. Boyle,⁵⁶ M.L. Brooks,³⁶ J. Bryslawskyj,^{5,8} V. Bumazhnov,²³ S. Campbell,^{13,27} C.-H. Chen,⁵⁶ D. Chen,⁶¹ M. Chiu,⁷ C.Y. Chi,¹³ I.J. Choi,²⁴ J.B. Choi,^{29,*} T. Chujo,⁶⁴ Z. Citron,⁶⁷ M. Connors,^{19,56} R. Corliss,⁶¹ M. Csanád,¹⁶ T. Csörgő,^{41,68} T.W. Danley,⁵⁰ A. Datta,⁴⁷ M.S. Daugherty,¹ G. David,^{7,61} K. DeBlasio,⁴⁷ K. Dehmelt,⁶¹ A. Denisov,²³ A. Deshpande,^{56,61} E.J. Desmond,⁷ A. Dion,⁶¹ P.B. Diss,³⁹ V. Doomra,⁶¹ J.H. Do,⁶⁹ A. Drees,⁶¹ K.A. Drees,⁶ J.M. Durham,³⁶ A. Durum,²³ A. Enokizono,^{55,57} R. Esha,⁶¹ B. Fadem,⁴⁴ W. Fan,⁶¹ N. Feege,⁶¹ D.E. Fields,⁴⁷ M. Finger, Jr.,⁹ M. Finger,⁹ D. Firak,^{15,61} D. Fitzgerald,⁴² S.L. Fokin,³³ J.E. Frantz,⁵⁰ A. Franz,⁷ A.D. Frawley,¹⁸ P. Gallus,¹⁴ C. Gal,⁶¹ P. Garg,^{3,61} H. Ge,⁶¹ M. Giles,⁶¹ F. Giordano,²⁴ A. Glenn,³⁵ Y. Goto,^{55,56} N. Grau,² S.V. Greene,⁶⁶ M. Grosse Perdekamp,²⁴ T. Gunji,¹¹ T. Guo,⁶¹ T. Hachiya,^{55,56} J.S. Haggerty,⁷ K.I. Hahn,¹⁷ H. Hamagaki,¹¹ H.F. Hamilton,¹ J. Hanks,⁶¹ S.Y. Han,^{17,32} S. Hasegawa,²⁸ T.O.S. Haseler,¹⁹ K. Hashimoto,^{55,57} T.K. Hemmick,⁶¹ X. He,¹⁹ J.C. Hill,²⁷ A. Hodges,^{19,24} R.S. Hollis,⁸ K. Homma,²⁰ B. Hong,³² T. Hoshino,²⁰ N. Hotvedt,²⁷ J. Huang,⁷ K. Imai,²⁸ M. Inaba,⁶⁴ A. Iordanova,⁸ D. Isenhower,¹ D. Ivanishchev,⁵⁴ B.V. Jacak,⁶¹ M. Jezghani,¹⁹ X. Jiang,³⁶ Z. Ji,⁶¹ B.M. Johnson,^{7,19} D. Jouan,⁵² D.S. Jumper,²⁴ S. Kanda,¹¹ J.H. Kang,⁶⁹ G. Kasza,^{41,68} D. Kawall,⁴⁰ A.V. Kazantsev,³³ J.A. Key,⁴⁷ V. Khachatryan,⁶¹ A. Khanzadeev,⁵⁴ B. Kimelman,⁴⁴ C. Kim,³² D.J. Kim,³⁰ E.-J. Kim,²⁹ G.W. Kim,¹⁷ M. Kim,⁵⁹ E. Kistenev,⁷ R. Kitamura,¹¹ J. Klatsky,¹⁸ D. Kleinjan,⁸ P. Kline,⁶¹ T. Koblesky,¹² B. Komkov,⁵⁴ D. Kotov,^{54,58} L. Kovacs,¹⁶ K. Kurita,⁵⁷ M. Kurosawa,^{55,56} Y. Kwon,⁶⁹ J.G. Lajoie,^{27,51} D. Larionova,⁵⁸ A. Lebedev,²⁷ S. Lee,⁶⁹ S.H. Lee,^{27,61} M.J. Leitch,³⁶ S.H. Lim,⁶⁹ M.X. Liu,³⁶ X. Li,¹⁰ X. Li,³⁶ D.A. Loomis,⁴² D. Lynch,⁷ S. Lökös,⁶⁸ Y.I. Makdisi,⁶ M. Makek,⁷⁰ A. Manion,⁶¹ V.I. Manko,³³ E. Mannel,⁷ M. McCumber,³⁶ P.L. McGaughey,³⁶ D. McGlinchey,^{12,36} C. McKinney,²⁴ A. Meles,⁴⁸ M. Mendoza,⁸ A.C. Mignerey,³⁹ A. Milov,⁶⁷ D.K. Mishra,⁴ J.T. Mitchell,⁷ M. Mitrankova,^{58,61} Iu. Mitrankov,^{58,61} S. Miyasaka,^{55,63} S. Mizuno,^{55,64} A.K. Mohanty,⁴ P. Montuenga,²⁴ T. Moon,^{32,69} D.P. Morrison,⁷ T.V. Moukhanova,³³ B. Mulilo,^{32,55,71} T. Murakami,^{34,55} J. Murata,^{55,57} A. Mwai,⁶⁰ K. Nagashima,²⁰ J.L. Nagle,¹² M.I. Nagy,¹⁶ I. Nakagawa,^{55,56} H. Nakagomi,^{55,64} K. Nakano,^{55,63} C. Nattress,⁶² P.K. Netrakanti,⁴ T. Niida,⁶⁴ S. Nishimura,¹¹ R. Nouicer,^{7,56} N. Novitzky,^{30,61} T. Novák,^{41,68} G. Nukazuka,^{55,56} A.S. Nyanin,³³ E. O'Brien,⁷ C.A. Ogilvie,²⁷ J.D. Orjuela Koop,¹² M. Orosz,^{15,22} J.D. Osborn,^{42,51} A. Oskarsson,³⁷ K. Ozawa,^{31,64} R. Pak,⁷ V. Pantuev,²⁵ V. Papavassiliou,⁴⁸ J.S. Park,⁵⁹ S. Park,^{43,55,59,61} M. Patel,²⁷ S.F. Pate,⁴⁸ J.-C. Peng,²⁴ D.V. Perepelitsa,^{7,12} G.D.N. Perera,⁴⁸ D.Yu. Peressounko,³³ J. Perry,²⁷ R. Petti,^{7,61} C. Pinkenburg,⁷ R. Pinson,¹ R.P. Pisani,⁷ M. Potekhin,⁷ M.L. Purschke,⁷ J. Rak,³⁰ B.J. Ramson,⁴² I. Ravinovich,⁶⁷ K.F. Read,^{51,62} D. Reynolds,⁶⁰ V. Riabov,^{46,54} Y. Riabov,^{54,58} D. Richford,^{5,65} T. Rinn,²⁷ S.D. Rolnick,⁸ M. Rosati,²⁷ Z. Rowan,⁵ J.G. Rubin,⁴² B. Sahlmueller,⁶¹ N. Saito,³¹ T. Sakaguchi,⁷ H. Sako,²⁸ V. Samsonov,^{46,54} M. Sarsour,¹⁹ S. Sato,²⁸ B. Schaefer,⁶⁶ B.K. Schmoll,⁶² K. Sedgwick,⁸ R. Seidl,^{55,56} A. Seleznev,⁵⁸ A. Sen,^{27,62} R. Seto,⁸ P. Sett,⁴ A. Sexton,³⁹ D. Sharma,⁶¹ I. Shein,²³ T.-A. Shibata,^{55,63} K. Shigaki,²⁰ M. Shimomura,^{27,45} P. Shukla,⁴ A. Sickles,^{7,24} C.L. Silva,³⁶ D. Silvermyr,^{37,51} B.K. Singh,³ C.P. Singh,^{3,*} V. Singh,³ M. Slunečka,⁹ K.L. Smith,^{18,36} M. Snowball,³⁶ R.A. Soltz,³⁵ W.E. Sondheim,³⁶ S.P. Sorensen,⁶² I.V. Sourikova,⁷ P.W. Stankus,⁵¹ M. Stepanov,^{40,*} S.P. Stoll,⁷ T. Sugitate,²⁰ A. Sukhanov,⁷ T. Sumita,⁵⁵ J. Sun,⁶¹ Z. Sun,^{15,22,61} J. Sziklai,⁶⁸ A. Taketani,^{55,56} K. Tanida,^{28,56,59} M.J. Tannenbaum,⁷ S. Tarafdar,^{66,67} A. Taranenko,^{46,60} R. Tieulent,^{19,38} A. Timilsina,²⁷ T. Todoroki,^{55,56,64} M. Tomášek,¹⁴ C.L. Towell,¹ R. Towell,¹ R.S. Towell,¹ I. Tserruya,⁶⁷ B. Ujvari,^{15,22} H.W. van Hecke,³⁶ J. Velkovska,⁶⁶ M. Virius,¹⁴ V. Vrba,^{14,26} X.R. Wang,^{48,56} Z. Wang,⁵ Y. Watanabe,^{55,56} Y.S. Watanabe,^{11,31} F. Wei,⁴⁸ A.S. White,⁴² C.L. Woody,⁷ M. Wysocki,⁵¹ B. Xia,⁵⁰ L. Xue,¹⁹ S. Yalcin,⁶¹ Y.L. Yamaguchi,^{11,61} A. Yanovich,²³ I. Yoon,⁵⁹ J.H. Yoo,³² I.E. Yushmanov,³³ H. Yu,^{48,53} W.A. Zajc,¹³ A. Zelenski,⁶ S. Zhou,¹⁰ and L. Zou⁸

(PHENIX Collaboration)

¹Abilene Christian University, Abilene, Texas 79699, USA

²Department of Physics, Augustana University, Sioux Falls, South Dakota 57197, USA

³Department of Physics, Banaras Hindu University, Varanasi 221005, India

⁴Bhabha Atomic Research Centre, Bombay 400 085, India

⁵Baruch College, City University of New York, New York, New York, 10010 USA

⁶Collider-Accelerator Department, Brookhaven National Laboratory, Upton, New York 11973-5000, USA

⁷Physics Department, Brookhaven National Laboratory, Upton, New York 11973-5000, USA

- ⁸ *University of California-Riverside, Riverside, California 92521, USA*
- ⁹ *Charles University, Faculty of Mathematics and Physics, 180 00 Troja, Prague, Czech Republic*
- ¹⁰ *Science and Technology on Nuclear Data Laboratory, China Institute of Atomic Energy, Beijing 102413, People's Republic of China*
- ¹¹ *Center for Nuclear Study, Graduate School of Science, University of Tokyo, 7-3-1 Hongo, Bunkyo, Tokyo 113-0033, Japan*
- ¹² *University of Colorado, Boulder, Colorado 80309, USA*
- ¹³ *Columbia University, New York, New York 10027 and Nevis Laboratories, Irvington, New York 10533, USA*
- ¹⁴ *Czech Technical University, Žitkova 4, 166 36 Prague 6, Czech Republic*
- ¹⁵ *Debrecen University, H-4010 Debrecen, Egyetem tér 1, Hungary*
- ¹⁶ *ELTE, Eötvös Loránd University, H-1117 Budapest, Pázmány P. s. 1/A, Hungary*
- ¹⁷ *Ewha Womans University, Seoul 120-750, Korea*
- ¹⁸ *Florida State University, Tallahassee, Florida 32306, USA*
- ¹⁹ *Georgia State University, Atlanta, Georgia 30303, USA*
- ²⁰ *Hiroshima University, Kagamiyama, Higashi-Hiroshima 739-8526, Japan*
- ²¹ *Department of Physics and Astronomy, Howard University, Washington, DC 20059, USA*
- ²² *HUN-REN ATOMKI, H-4026 Debrecen, Bem tér 18/c, Hungary*
- ²³ *IHEP Protvino, State Research Center of Russian Federation, Institute for High Energy Physics, Protvino, 142281, Russia*
- ²⁴ *University of Illinois at Urbana-Champaign, Urbana, Illinois 61801, USA*
- ²⁵ *Institute for Nuclear Research of the Russian Academy of Sciences, prospekt 60-letiya Oktyabrya 7a, Moscow 117312, Russia*
- ²⁶ *Institute of Physics, Academy of Sciences of the Czech Republic, Na Slovance 2, 182 21 Prague 8, Czech Republic*
- ²⁷ *Iowa State University, Ames, Iowa 50011, USA*
- ²⁸ *Advanced Science Research Center, Japan Atomic Energy Agency, 2-4 Shirakata Shirane, Tokai-mura, Naka-gun, Ibaraki-ken 319-1195, Japan*
- ²⁹ *Jeonbuk National University, Jeonju, 54896, Korea*
- ³⁰ *Helsinki Institute of Physics and University of Jyväskylä, P.O.Box 35, FI-40014 Jyväskylä, Finland*
- ³¹ *KEK, High Energy Accelerator Research Organization, Tsukuba, Ibaraki 305-0801, Japan*
- ³² *Korea University, Seoul 02841, Korea*
- ³³ *National Research Center "Kurchatov Institute", Moscow, 123098 Russia*
- ³⁴ *Kyoto University, Kyoto 606-8502, Japan*
- ³⁵ *Lawrence Livermore National Laboratory, Livermore, California 94550, USA*
- ³⁶ *Los Alamos National Laboratory, Los Alamos, New Mexico 87545, USA*
- ³⁷ *Department of Physics, Lund University, Box 118, SE-221 00 Lund, Sweden*
- ³⁸ *IPNL, CNRS/IN2P3, Univ Lyon, Université Lyon 1, F-69622, Villeurbanne, France*
- ³⁹ *University of Maryland, College Park, Maryland 20742, USA*
- ⁴⁰ *Department of Physics, University of Massachusetts, Amherst, Massachusetts 01003-9337, USA*
- ⁴¹ *MATE, Institute of Technology, Laboratory of Femtoscopy, Károly Róbert Campus, H-3200 Gyöngyös, Mátrai út 36, Hungary*
- ⁴² *Department of Physics, University of Michigan, Ann Arbor, Michigan 48109-1040, USA*
- ⁴³ *Mississippi State University, Mississippi State, Mississippi 39762, USA*
- ⁴⁴ *Muhlenberg College, Allentown, Pennsylvania 18104-5586, USA*
- ⁴⁵ *Nara Women's University, Kita-uoya Nishi-machi Nara 630-8506, Japan*
- ⁴⁶ *National Research Nuclear University, MEPhI, Moscow Engineering Physics Institute, Moscow, 115409, Russia*
- ⁴⁷ *University of New Mexico, Albuquerque, New Mexico 87131, USA*
- ⁴⁸ *New Mexico State University, Las Cruces, New Mexico 88003, USA*
- ⁴⁹ *Physics and Astronomy Department, University of North Carolina at Greensboro, Greensboro, North Carolina 27412, USA*
- ⁵⁰ *Department of Physics and Astronomy, Ohio University, Athens, Ohio 45701, USA*
- ⁵¹ *Oak Ridge National Laboratory, Oak Ridge, Tennessee 37831, USA*
- ⁵² *IPN-Orsay, Univ. Paris-Sud, CNRS/IN2P3, Université Paris-Saclay, BP1, F-91406, Orsay, France*
- ⁵³ *Peking University, Beijing 100871, People's Republic of China*
- ⁵⁴ *PNPI, Petersburg Nuclear Physics Institute, Gatchina, Leningrad region, 188300, Russia*
- ⁵⁵ *RIKEN Nishina Center for Accelerator-Based Science, Wako, Saitama 351-0198, Japan*
- ⁵⁶ *RIKEN BNL Research Center, Brookhaven National Laboratory, Upton, New York 11973-5000, USA*
- ⁵⁷ *Physics Department, Rikkyo University, 3-34-1 Nishi-Ikebukuro, Toshima, Tokyo 171-8501, Japan*
- ⁵⁸ *Saint Petersburg State Polytechnic University, St. Petersburg, 195251 Russia*
- ⁵⁹ *Department of Physics and Astronomy, Seoul National University, Seoul 151-742, Korea*
- ⁶⁰ *Chemistry Department, Stony Brook University, SUNY, Stony Brook, New York 11794-3400, USA*
- ⁶¹ *Department of Physics and Astronomy, Stony Brook University, SUNY, Stony Brook, New York 11794-3800, USA*
- ⁶² *University of Tennessee, Knoxville, Tennessee 37996, USA*
- ⁶³ *Department of Physics, Tokyo Institute of Technology, Oh-okayama, Meguro, Tokyo 152-8551, Japan*
- ⁶⁴ *Tomonaga Center for the History of the Universe, University of Tsukuba, Tsukuba, Ibaraki 305, Japan*
- ⁶⁵ *United States Merchant Marine Academy, Kings Point, New York 11024, USA*
- ⁶⁶ *Vanderbilt University, Nashville, Tennessee 37235, USA*
- ⁶⁷ *Weizmann Institute, Rehovot 76100, Israel*
- ⁶⁸ *Institute for Particle and Nuclear Physics, HUN-REN Wigner Research Centre for Physics, (HUN-REN Wigner RCP, RMI), H-1525 Budapest 114, POBox 49, Budapest, Hungary*

⁶⁹Yonsei University, IPAP, Seoul 120-749, Korea

⁷⁰Department of Physics, Faculty of Science, University of Zagreb, Bijenička c. 32 HR-10002 Zagreb, Croatia

⁷¹Department of Physics, School of Natural Sciences, University of Zambia, Great East Road Campus, Box 32379, Lusaka, Zambia

(Dated: April 7, 2025)

The PHENIX experiment at the Relativistic Heavy Ion Collider measured the second Fourier component v_2 of the direct-photon azimuthal anisotropy at midrapidity in Au+Au collisions at $\sqrt{s_{NN}} = 200$ GeV. The results are presented in 10% wide bins of collision centrality and cover the transverse-momentum range of $1 < p_T < 20$ GeV/c, and are in quantitative agreement with findings published earlier, but provide better granularity and higher p_T reach. Above a p_T of 8–10 GeV/c, where hard scattering dominates the direct-photon production, v_2 is consistent with zero. Below that in each centrality bin v_2 as a function of p_T is comparable to the π^0 anisotropy albeit with a tendency of being somewhat smaller. The results are compared to recent theory calculations that include, in addition to thermal radiation from the quark-gluon plasma and hadron gas, sources of photons from pre-equilibrium, strong magnetic fields, or radiative hadronization. While the newer theoretical calculations describe the data better than previous models, none of them alone can fully explain the results, particularly in the region of $p_T = 4$ –8 GeV/c.

I. INTRODUCTION

The quark-gluon plasma (QGP) is a deconfined state of quarks and gluons that arises from the principles of asymptotic freedom in quantum chromodynamics, the theory of strong interactions. Since the establishment of the Relativistic Heavy Ion Collider (RHIC) in the early 2000s, the formation of QGP has been well-documented in relativistic heavy-ion collisions [1–4]. Photons serve as a unique probe for studying the space-time evolution of these collisions [5] as their mean free path is larger than the system size and, hence, carry unaltered information about the dynamics of the system as it explosively expands and cools. The photons of interest, those that do not originate from hadron decays, are referred to as direct photons. Sources of direct photons, ordered by emission time, include (a) prompt photons produced in early hard-scattering processes [6–8], (b) a number of possible mechanisms emitting photons before QGP is formed, such as pre-equilibrium phase [9], the hot-gluon scenario [10], the Glasma state [11], the strong magnetic field created in off-central collisions [12] etc, and (c) radiation from the fireball of the QGP phase through hadronization until kinetic freezeout of hadrons [8, 9, 13–18]; and final-state effects, such as jet-medium interactions [19, 20].

Measurements of direct photons at RHIC [21–29] and the Large Hadron Collider [30, 31] constrain initial conditions, sources of photon production, emission rates, and the space-time evolution of relativistic heavy-ion collisions. In general, theoretical models are qualitatively consistent with the observed large yields, azimuthal anisotropy, and centrality dependence. However, they do not describe the details of the data quantitatively (for a review see [32]).

This study focuses on the azimuthal anisotropy of direct-photon emission, which is highly sensitive to the

initial state of the fireball. Even slight modifications can lead to significant variations in the final-state results [33]. Anisotropies arise in off-center heavy-ion collisions, which create an elliptical interaction region, generating pressure gradients along the surface. These pressure gradients drive an anisotropic expansion of the fireball [34]. Photons emitted from the fireball will experience an anisotropic blue shift [8, 13–15, 35–37], depending on the time of emission. Prompt and early photons will be largely unaffected, while photons from the expanding hadron gas (HG) will experience the largest blue shifts and thus the largest anisotropies. Other sources of anisotropies may exist. For example, the strong, polarized electromagnetic fields created during heavy-ion collisions might alter emission rates early in the collisions [38–41]. These changes will depend on the direction relative to the polarization of the fields, thereby creating an anisotropy with respect to the reaction plane. Also photon emission influenced by final-state effects, such as jet quenching, will be altered differently depending on the path length through the medium; again resulting in an anisotropy [19, 20].

The quantity measured, in this context, is the Fourier transform of the azimuthal distribution of photons [42, 43], which can be written as

$$\frac{dN}{dp_T d(\phi - \Psi_k)} \propto 1 + \sum_n v_{n,k} \cos(n(\phi - \Psi_k)), \quad (1)$$

where ϕ is the azimuthal angle in the global coordinate system, and Ψ_k is the orientation of the k -th order event plane in the given event, estimated from the distribution of particles in a forward event-plane detector. The coefficients $v_{n,k}$ are the n -th harmonic with respect to the k -th reaction plane. Except for the $k = 2$ event plane, which is to first order the reaction plane, all other planes result from density fluctuations in the incoming beams. Statistics limits this study to the $k = 2$ event plane with the leading coefficient $v_{2,2} \equiv v_2\{\Psi_2\}$, which we will refer to as v_2 , and a minor contribution from $v_{4,2} \equiv v_4\{\Psi_2\}$,

* Deceased

† PHENIX Spokesperson: akiba@rcf.rhic.bnl.gov

which we will refer to as v_4 .

In this paper, the PHENIX collaboration reports the measurement of v_2 for direct photons in Au+Au collisions at RHIC at $\sqrt{s_{NN}} = 200$ GeV using the high-statistics data collected in 2014. Section II describes the experimental setup, followed by data analysis in Section III. Sources of systematic uncertainties are presented in Section IV, and results are discussed in Sections V and VI. Finally, a summary is given in Section VII

II. EXPERIMENTAL SETUP AND PHOTON MEASUREMENTS

In 2014, PHENIX recorded 1.9×10^{10} Au+Au collisions or events at $\sqrt{s_{NN}} = 200$ GeV with the detector setup shown in Fig. 1. Of these 1.25×10^{10} events passed all quality and selection cuts in the present analysis. Collisions were identified by a minimum-bias trigger that requires coincident signals in two beam-beam counters (BBC) [44] that are located on either side of the interaction point along the beam axis at $z = \pm 1.44$ m. Each BBC is segmented into 64 Čerenkov counters that measure the number of produced charged particles and their arrival time in $3.1 < |\eta| < 3.9$. The timing information provides the trigger and the z -position of the collision vertex along the beam direction with a resolution of less than a centimeter. Only events that occurred within ± 10 cm of the nominal interaction point are analyzed. The particle multiplicity information is used to divide events into 10% centrality classes.

The direct photon measurement is performed using the electromagnetic calorimeters (EMCal) [45] in the central-arm spectrometers. Each arm has 4 sectors covering a total of $2 \times 90^\circ$ in azimuth and $|\eta| < 0.35$. Two types of calorimeters are used: 6 sectors are lead-scintillator (PbSc) sampling EMCal and 2 are lead-glass (PbGl) EMCal, which provide energy resolutions of $\sigma_E/E = 8.1\%/\sqrt{E} [\text{GeV}] \oplus 5.0\%$, and $\sigma_E/E = 8.7\%/\sqrt{E} [\text{GeV}] \oplus 5.8\%$, respectively. Photon identification is accomplished through cuts on shower shape, comparing the reconstructed showers to template electromagnetic showers. A match of $\chi^2 < 3$ is required. The selected photon sample covers a range of $0.5 < p_T < 20$ GeV/ c .

The event plane, Ψ_2 , is measured with the two forward-vertex (FVTX) detectors [46] of the PHENIX silicon-vertex tracker. The FVTX extends the vertex tracking to the range of $1.2 < |\eta| < 2.2$ (for tracks) and $1.0 < |\eta| < 3.0$ (for clusters) and 2π in azimuth. Each side has 4 stations in the beam direction with 48 individual silicon sensors. Each sensor contains two columns of ministrips with $75 \mu\text{m}$ pitch in the radial direction and lengths in the azimuthal direction varying from 3.4 mm at the inner radius to 11.5 mm at the outer radius. The FVTX has approximately 0.54 million strips on each side. Ψ_2 can be measured with a resolution of up to 75% for semicentral events.

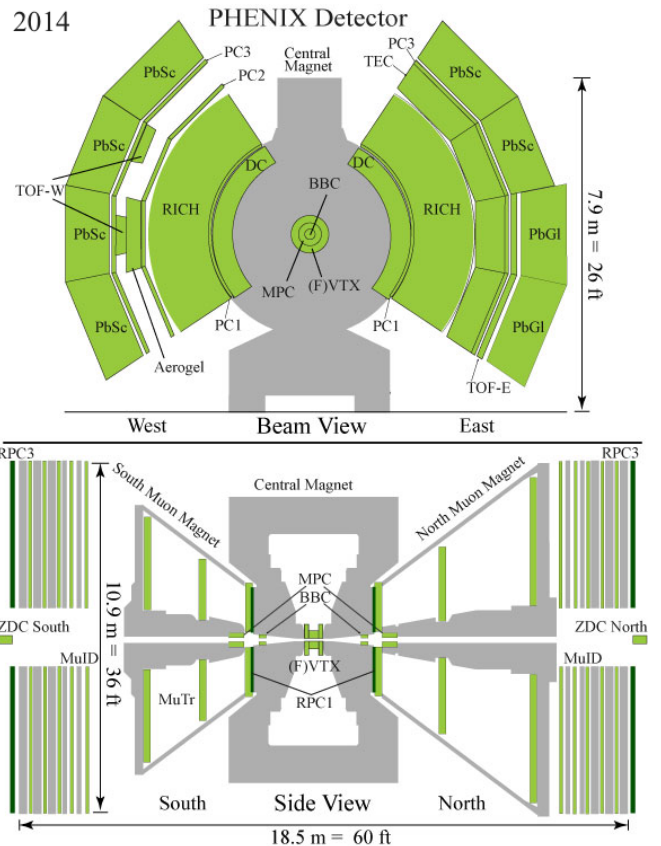


FIG. 1. Beam view and side view of the PHENIX detector setup for the year 2014.

III. DATA ANALYSIS

The azimuthal anisotropy of direct photons v_2^{dir} with respect to the event plane Ψ_2 is calculated from the measured anisotropy of all photon candidates v_2^{inc} and that of modeled photons from hadron decays v_2^{dec} . Using the fraction R_γ of the inclusive photon yield divided by the yield of decay photons, the direct-photon anisotropy can be calculated as

$$v_2^{\text{dir}} = \frac{R_\gamma v_2^{\text{inc}} - v_2^{\text{dec}}}{R_\gamma - 1}. \quad (2)$$

where all quantities are functions of photon p_T . Each term in Eq. 2 and Ψ_2 are determined separately.

A. The event plane Ψ_2

The reaction plane of a collision is the plane defined by the intersection of the beam direction with the impact parameter of the two colliding nuclei. However, this is experimentally inaccessible. It is instead estimated using the event plane Ψ_2 [43, 47] measured from the distribution of particles detected in the FVTX.

The orientation of the event plane Ψ_2 in global coordinates is calculated using the azimuthal distribution of the charged particle tracks reconstructed in the FVTX for a given event. The components of the event-plane vector Q are defined as Q_x and Q_y :

$$Q_x = \sum_i \cos(2\phi_i), \quad Q_y = \sum_i \sin(2\phi_i), \quad (3)$$

where (ϕ_i) is the azimuthal angle of the (i -th) particle. The event-plane Ψ_2 is then calculated as:

$$\Psi_2 = \frac{1}{2} \arctan\left(\frac{Q_y}{Q_x}\right). \quad (4)$$

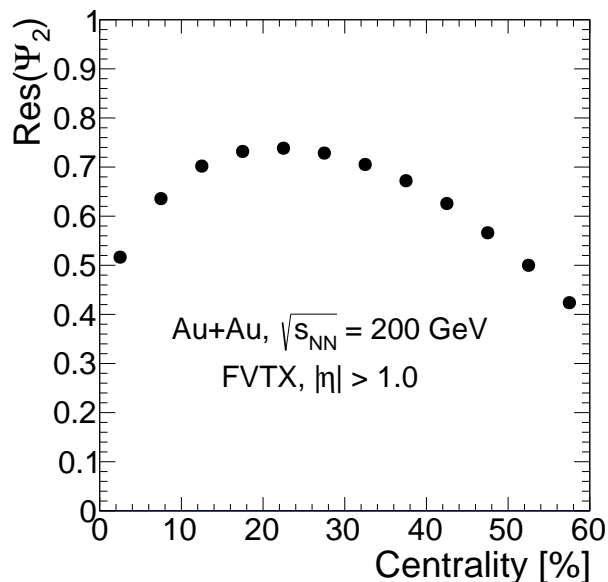


FIG. 2. The event-plane resolution for different centralities using the three subevent method.

The event-plane resolution $\text{Res}(\Psi_2)$ is calculated using the combinations of three subevents. In this approach, the event-plane angles from three independent detector regions are compared. The resolution factor is given by

$$\text{Res}(\Psi_2) = \sqrt{\frac{\langle \cos(2[\Psi_2^A - \Psi_2^B]) \rangle \langle \cos(2[\Psi_2^A - \Psi_2^C]) \rangle}{\langle \cos(2[\Psi_2^B - \Psi_2^C]) \rangle}}, \quad (5)$$

where Ψ_2^A , Ψ_2^B , and Ψ_2^C are the event planes determined from (A) tracks in the FVTX, (B) hits in the BBC detector, and (C) tracks reconstructed in the central-arm detectors. The event-plane resolution is shown in Fig. 2 as a function of centrality. The event-plane resolution depends on the number of charged particles produced in a collision and the size of the anisotropy of the charged-particle production for a given centrality class. This leads

to a broad maximum near semicentral collisions, where $\text{Res}(\Psi_2)$ reaches $\approx 75\%$. Towards more central collisions it reduces to $\approx 50\%$; and as collisions become more peripheral the resolution drops to $\approx 40\%$.

B. Inclusive photon anisotropy v_2^{inc}

Showers in the EMCal are identified as photon candidates by comparing the shower shape to templates of electromagnetic showers using a $\chi^2 < 3$ match. For a given centrality and p_T -range, the anisotropy of all photon candidates is measured directly by fitting the distribution of azimuthal angles, ϕ , of the photons relative to the event plane Ψ_2 . The functional form of the fit is given as

$$\frac{dN}{d\Delta\phi} = \left\langle \frac{dN}{d\phi} \right\rangle (1 + 2v_2 \cos(2\Delta\phi) + 2v_4 \cos(4\Delta\phi)), \quad (6)$$

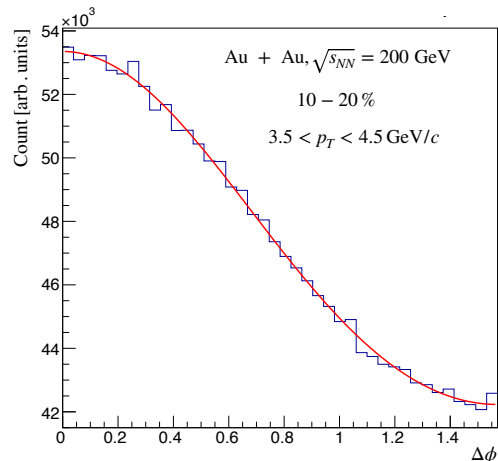


FIG. 3. Sample plot of $dN/d\Delta\phi$ vs $\Delta\phi$. The red line is the cosine fit used to determine v_2 .

where $\Delta\phi = \phi - \Psi_2$. An example is shown in Fig. 3. The extracted parameter v_2 underestimates the actual v_2^{inc} because of the finite event-plane resolution. To obtain v_2^{inc} , v_2 needs to be corrected with

$$v_2^{\text{inc}} = \frac{v_2}{\text{Res}(\Psi_2)}. \quad (7)$$

C. Decay photon anisotropy v_2^{dec}

The modeling of v_2^{dec} is based on a fast simulation of π^0 , η , ω , and η' using the PHENIX decay generator, which simulates mesons according to given input p_T spectra; decays them based on the known decay kinematics and branching ratios; and aggregates the decay photons in the PHENIX-detector acceptance.

The mesons are generated with $0.1 < p_T < 25$ GeV/c, $|y| < 0.5$ and 2π in azimuth. The p_T distribution for π^0 is based on experimental data [48–50] fitted by a modified Hagedorn function:

$$\frac{1}{2\pi p_T} \frac{dN}{dp_T} = A \left(e^{-am_T - bm_T^2} + \frac{m_T}{p_0} \right)^{-n}, \quad (8)$$

$$m_T = \sqrt{p_T^2 + m^2 - m_{\pi^0}^2}, \quad (9)$$

where the parameters A , a , b , p_0 , n for π^0 are given in Table I.

TABLE I. Parameters for π^0 for the modified Hagedorn function Eq. 8 to PHENIX data [48–50] from Au+Au collisions at $\sqrt{s_{NN}} = 200$ GeV.

centrality	A (GeV/c) ⁻²	a (GeV/c) ⁻¹	b (GeV/c) ⁻²	p_0 GeV/c	n
min.bias	504.5	0.5169	0.1626	0.7366	8.274
0%–10%	1331.0	0.5654	0.1945	0.7429	8.361
10%–20%	1001.0	0.5260	0.1628	0.7511	8.348
20%–30%	750.7	0.4900	0.1506	0.7478	8.229
30%–40%	535.3	0.4534	0.1325	0.7525	8.333
40%–50%	364.5	0.4333	0.1221	0.7385	8.261
50%–60%	231.2	0.4220	0.1027	0.7258	8.220
60%–70%	118.1	0.4416	0.0559	0.7230	8.163
70%–80%	69.2	0.2850	0.0347	0.7787	8.532
80%–93%	51.1	0.2470	0.0619	0.7101	8.453

For η , the p_T spectra are derived by scaling the π^0 spectra with the η/π^0 ratio, as detailed in [51]

$$E \frac{d^3 N_\eta}{dp^3} = E \frac{d^3 N_{\pi^0}}{dp^3} \times \eta/\pi^0 \times R_{\text{flow}}, \quad (10)$$

where R_{flow} accounts for radial-flow effects, calculated as the ratio of K^\pm/π^\pm in Au+Au collisions to that in $p+p$ collisions. This method incorporates world data for η/π^0 and avoids the over-estimation from m_T -scaling. The momentum distributions for ω and η' are obtained from m_T -scaling using Eq. 9. The normalization of ω and η' are fixed at $p_T = 5$ GeV/c to 0.9 ± 0.06 and 0.25 ± 0.075 , respectively [24].

The p_T distributions are modulated with v_2 . For π^0 the v_2 is based on experimental data from Au+Au collisions at $\sqrt{s_{NN}} = 200$ GeV for charged pions [52] and neutral pions [53]. An empirical functional form, given by

$$\frac{v_2}{n_q} = N_1 \tan^{-1}(\alpha x) + N_2(x^2 + \beta x)e^{-\lambda x}, \quad (11)$$

$$x = \frac{1}{n_q} \left(\sqrt{p_T^2 + m^2} - m \right) = KE_T, \quad (12)$$

is fitted to the data, where the fit parameters are N_1 , α , N_2 , β , and λ ; n_q is the number of valence quarks in the particle ($n_q = 2$ for mesons); KE_T is the transverse kinetic energy; and m is the particle mass. The shape was chosen so that v_2 is zero at $p_T = 0$ and a constant asymptotic value at high p_T , while allowing for a maximum at medium p_T . An example is shown in Fig. 4. Here and in all following figures statistical uncertainties are shown as error bars, while systematic uncertainties are shown as shaded bars or bands.

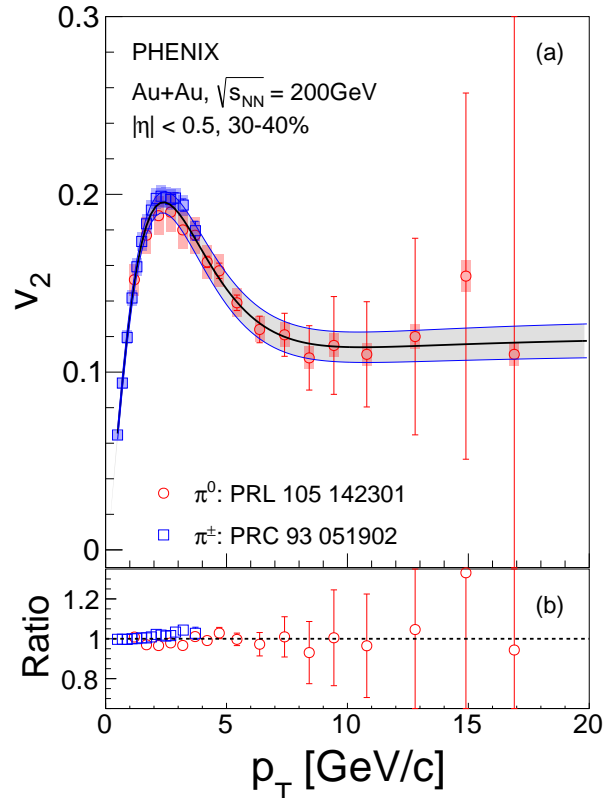


FIG. 4. Combined fit for neutral and charged pion v_2 data sets as a function of p_T ; statistical errors are shown as bars, systematic uncertainties as shaded area. The upper and lower bounds of the fit, shown as band, are determined by an MC sampling method.

The v_2 of heavier mesons is assumed to follow the same functional form as pions, scaled with KE_T according to mass differences [52]:

$$v_2(KE_T^{\pi^0}) = v_2(KE_T^{\eta,\omega,\eta'}). \quad (13)$$

In the next step, all mesons are decayed to final states containing photons, weighted by their branching ratios. The photons are aggregated in bins of p_T and for each bin the $dN/d\phi$ distribution is fitted to determine v_2^{dec} .

D. Determination of R_γ

Finally, the ratio R_γ , which is the inclusive photon yield divided by the photon yield from hadron decays, is needed to appropriately weight the inclusive-photon contribution in Eq. 2. The ratio R_γ is determined from a combined fit to data previously published by PHENIX for Au+Au collisions at $\sqrt{s_{NN}} = 200$ GeV [23, 29]. The data for 10% centrality bins are fitted with an empirical functional form:

$$R_\gamma(p_T) = M_0 + \frac{M_1}{1 + e^{m_0(p_T - m_1)}}, \quad (14)$$

where M_0 , M_1 , m_0 , and m_1 are the fit parameters. A representative plot of R_γ versus p_T , along with the fitted curve and systematic uncertainties, is shown in Fig. 5. The functional form has no direct physical meaning, but was chosen to give a good representation of the data with the following features. The value of R_γ is approximately 1.15 at $p_T \approx 1$ GeV/c, for all centrality ranges studied here. R_γ then increases monotonically over the entire p_T range and saturates at very high p_T . The value at $p_T \approx 18$ GeV/c increases with centrality, consistent with the larger suppression of π^0 in more central collisions and the absence of a nuclear modification for prompt photons.

TABLE II. Absolute systematic uncertainties on v_2^{dir} . Values shown are selected p_T and centralities. Positive and negative uncertainties are averaged here, but shown separately in Figs. 7–9. In addition to the total uncertainty on v_2^{dir} , also given are the individual contributions due to uncertainties on R_γ , v_2^{inc} , and v_2^{dec} , which are calculated using the same sampling method but setting the other uncertainties to zero.

Uncertainty	centrality	p_T [GeV/c]			
on v_2^{dir} due to		2.5	5	10	15
total	0%–10%	0.023	0.018	0.015	0.025
	30%–40%	0.05	0.03	0.035	0.06
	50%–60%	0.08	0.08	0.06	0.09
R_γ	0%–10%	0.003	0.003	0.003	0.005
	30%–40%	0.01	0.01	0.015	0.015
	50%–60%	0.025	0.025	0.025	0.025
v_2^{inc}	0%–10%	0.016	0.016	0.014	0.023
	30%–40%	0.04	0.024	0.03	0.06
	50%–60%	0.035	0.037	0.04	0.08
v_2^{dec}	0%–10%	0.018	0.01	0.005	0.005
	30%–40%	0.037	0.019	0.011	0.009
	50%–60%	0.09	0.07	0.05	0.03

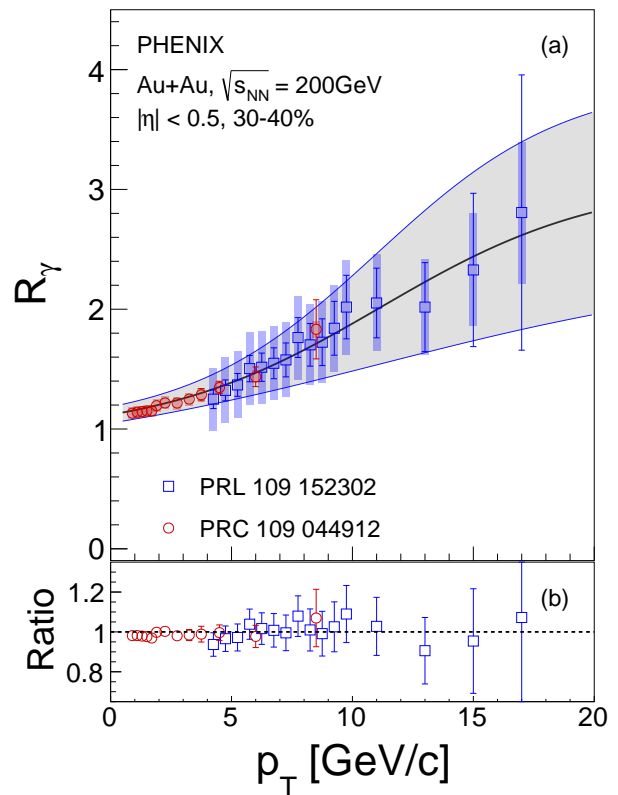


FIG. 5. Sample plot of R_γ vs. p_T ; statistical errors of the data are shown as bars, systematic uncertainties as shaded area. The fit, obtained using the Monte Carlo sampling procedure, is given with systematic uncertainties shown as band.

IV. SYSTEMATIC UNCERTAINTIES

The systematic uncertainties on v_2^{dir} are calculated from the individual uncertainties on v_2^{inc} , v_2^{dec} , and R_γ . Typical values are presented in Table II. There are multiple sources of uncertainty on each of these quantities.

The v_2^{inc} for the inclusive-photon yield is determined from the yield of photon candidates, which is not corrected for detector effects. This is based on the premise that the photon reconstruction efficiency does not depend on $\Delta\phi$, the angle of the photon with respect to the event plane Ψ_2 , and is independent of the source of the photons. The latter is only true if the showers of two decay photons do not overlap.

The uniformity and independence of the reconstruction efficiency with respect to the reaction plane is estimated by comparing results obtained using only the EMCAL in the east and west arms respectively. The difference in v_2^{inc} is 2%–7%, depending on p_T and centrality. There are also uncertainties on v_2^{inc} due to the accuracy with which the event plane can be determined. This is estimated by comparing different subevent combinations and found

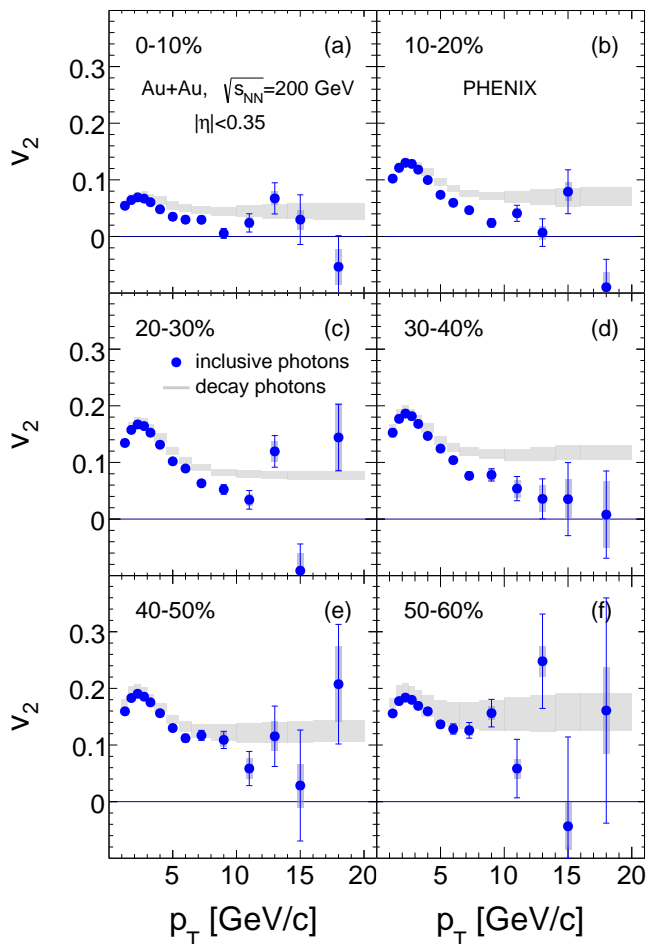


FIG. 6. Comparison of the measured anisotropy of inclusive photon production v_2^{inc} and the modeled anisotropy for photons from hadron decay v_2^{dec} . Panels (a) through (f) represent 10% centrality selections from central to semiperipheral collisions. Statistical uncertainties on v_2^{inc} are shown as error bars, while systematic uncertainties are shown as shaded bars. For v_2^{dec} a band covering the possible systematic variations is given.

to be 1%–5%. The effect of shower merging is negligible below a photon p_T of 10 GeV/c, but the inclusive photon yield from 10 to 20 GeV/c gradually decreases by up to 10%, as more and more of the showers from $\pi^0 \rightarrow \gamma\gamma$ decay photons overlap.

Imperfections due to incomplete suppression of the hadron contamination in the inclusive-photon sample are estimated by varying the photon-identification cuts. The analysis was repeated using different identification cuts and the variation of the results was used as a measure to estimate the uncertainty, determined to be $\approx 2\%$.

The uncertainties on v_2^{dec} are dominated by the uncertainties on the determination of v_2 for π^0 . These are determined through the fitting procedure, which uses a Monte-Carlo sampling technique. In this approach, each data point is given a Gaussian distribution according to

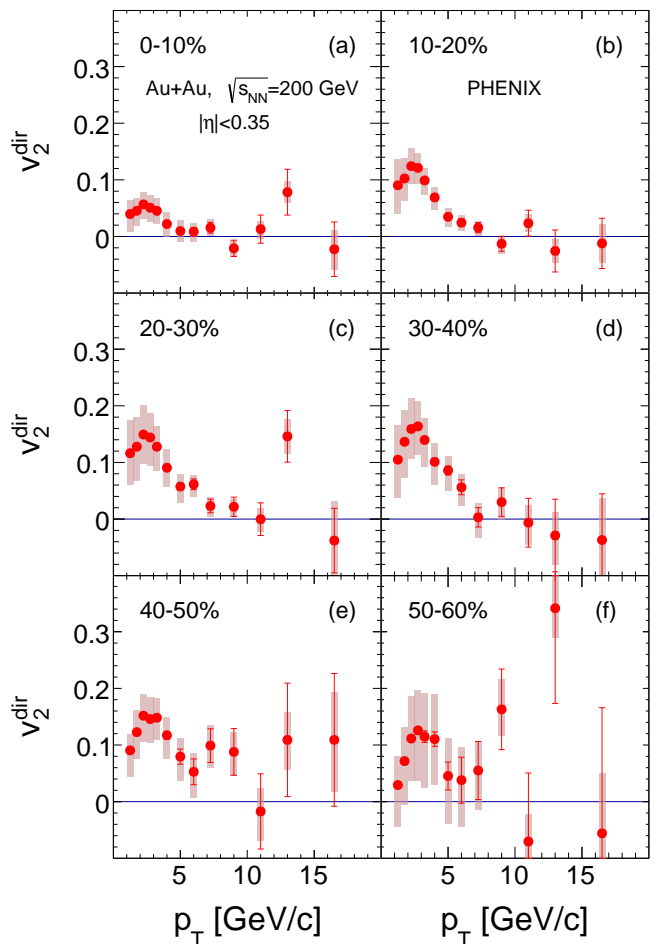


FIG. 7. Anisotropy of direct-photon production v_2^{dir} . Panels (a) through (f) represent 10% centrality selections from central to semiperipheral collisions. Statistical uncertainties on v_2^{dir} are shown as error bars, while systematic uncertainties are shown as shaded bars.

its statistical uncertainty, and varied independently. All data points of a given data set are also varied simultaneously within their correlated systematic uncertainties. The resulting uncertainties, shown as bands in Fig. 6, are largest at high p_T and for the semiperipheral bin where they reach 25%. The additional uncertainty on $v_2^{\pi^0}$ arising from the event-plane determination is $\approx 3\%$. The contributions to v_2^{dec} from other mesons are small, and the uncertainties introduced by the KE_T scaling are estimated to be 2%. Other uncertainties are negligible.

Finally, the uncertainties on R_γ are estimated through the fitting procedure, similar to the process used for the $v_2^{\pi^0}$ uncertainties. An example is given as the band in Fig. 5. Depending on p_T and centrality the uncertainties are estimated to vary from 5% to 30%. Most uncertainties are correlated across different centrality ranges. The uncertainty from the event-plane determination is a scale uncertainty, while all other uncertainties are correlated in p_T .

The v_2^{dir} is calculated from v_2^{inc} , v_2^{dec} , and R_γ using Eq. 2. Due to the nonlinear dependence on R_γ , uncertainties are asymmetric unless $v_2^{\text{inc}} = v_2^{\text{dec}}$. To address this, the sampling procedure developed in [25] was applied. Each component of the calculation of v_2^{dir} is modeled as a Gaussian distribution with its uncertainty as the width. Using these distributions, many calculations of v_2^{dir} are performed, producing a probability distribution for v_2^{dir} . Asymmetric systematic uncertainties are determined from $\Delta_{v_2^{\text{dir}}}^+$ and $\Delta_{v_2^{\text{dir}}}^-$, the difference between the two v_2^{dir} values where the probability reaches half of the maximum value to the v_2^{dir} value at the maximum probability. The uncertainties are quoted as $2\Delta_{v_2^{\text{dir}}}^\pm/2.35$.

V. RESULTS

The values of the inclusive photon anisotropy v_2^{inc} and the expected anisotropy v_2^{dec} of photons from hadron decays are compared in Fig. 6, which shows six 10% centrality classes from 0%–10% to 50%–60% of Au+Au collisions at $\sqrt{s_{\text{NN}}} = 200$ GeV. The p_T range extends from 1 to 20 GeV/c, which significantly increases the range previously accessible, $p_T < 5$ GeV/c [25] and 10 GeV/c [22]. For all p_T , v_2^{inc} is smaller than v_2^{dec} , however below 4 GeV/c the difference is small and within uncertainties. Above $p_T > 4$ GeV/c, v_2^{inc} is visibly lower than the v_2^{dec} for most cases, signaling a substantial contribution of direct photons from a source that does not exhibit an anisotropy with respect to the event plane. This is consistent with the expectation that prompt photon production would dominate in this p_T range and these photons are not expected to have an anisotropy.

The values of v_2^{dir} , calculated from v_2^{inc} , v_2^{dec} , and R_γ using Eq. 2, are depicted in Fig. 7. For $p_T < 4$ GeV/c, v_2^{dir} is large and very similar to v_2 observed for pions [52]. The value increases up to ≈ 2 –3 GeV/c, where it has a broad maximum. While v_2^{dir} decreases towards higher p_T , nonzero v_2^{dir} values seem to extend to well beyond 4 GeV/c in p_T . Only above 8–10 GeV/c, v_2^{dir} becomes consistent with zero.

The maximum value v_2^{dir} reaches is ≈ 0.16 for the semi-central event selection of 30%–40% centrality or $N_{\text{coll}} \approx 200$. The centrality dependence of the peak value is shown in Fig. 8(a). Although the systematic uncertainties are significant, because they are correlated, the data establish a decrease of v_2^{dir} towards higher and lower values of N_{coll} . At high $p_T > 10$ GeV/c, the direct-photon anisotropy is consistent with zero over the entire range from central to semiperipheral collisions with $N_{\text{coll}} \approx 50$, as seen in Fig. 8(b).

VI. DISCUSSION AND CONCLUSION

The data are consistent with previous publications [22, 52], as can be seen in Fig. 9, where the data are aggre-

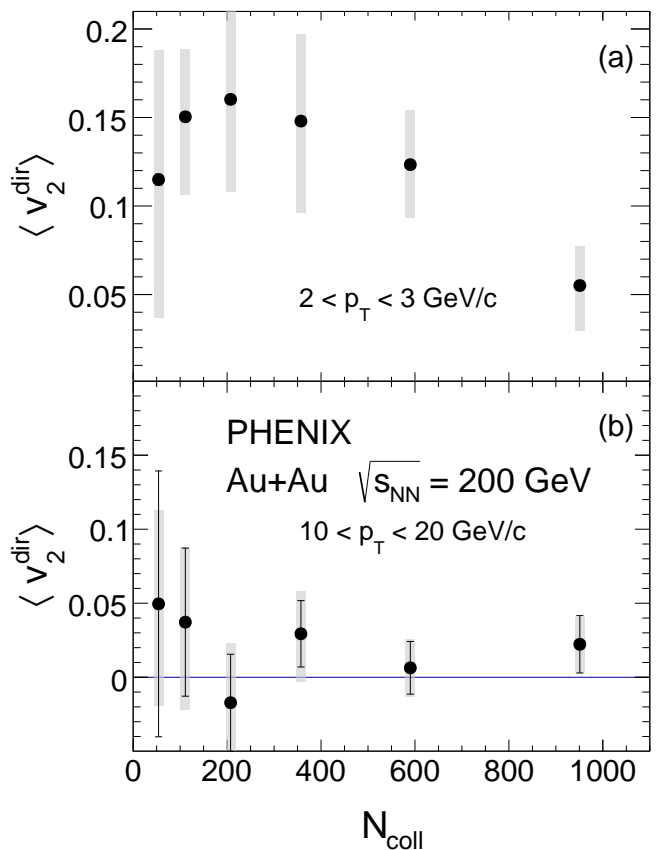


FIG. 8. Average azimuthal anisotropy for two different p_T ranges as a function of centrality, here represented by the number of binary nucleon-nucleon collisions N_{coll} . Panel (a) shows the range from 2 to 3 GeV/c where the anisotropy is maximal. Panel (b) shows the high p_T range from 10 to 20 GeV/c, where the photon is dominated by prompt production through hard scattering processes. For each point statistical errors are represented by lines, while systematic uncertainties are shown as shaded band.

gated for 0%–20% and 20%–40% centrality and compared directly to previously published data. For these two centrality bins also a number of theoretical calculations of the direct-photon anisotropy exist, covering the p_T range up to 5 GeV/c.

The value of v_2^{dir} reaches a maximum for all centralities ≈ 2 –3 GeV/c. Model calculations of thermal photons emitted from the rapidly expanding QGP and HG phases [8, 13–15, 35] also show a peak structure at similar p_T . A representative calculation of the QGP plus HG contributions [9], is shown in Fig. 9 to illustrate this point. However, the values of v_2^{dir} and the direct-photon yields associated with them are generally found to be too low [52] to explain the data. This mismatch is part of the “direct-photon puzzle” [32].

In the multimessenger approach [9], contributions from the pre-equilibrium stage have been added to those of the QGP and HG, seen in Fig. 9 as the dotted line. While these contributions can increase the anisotropy and seem

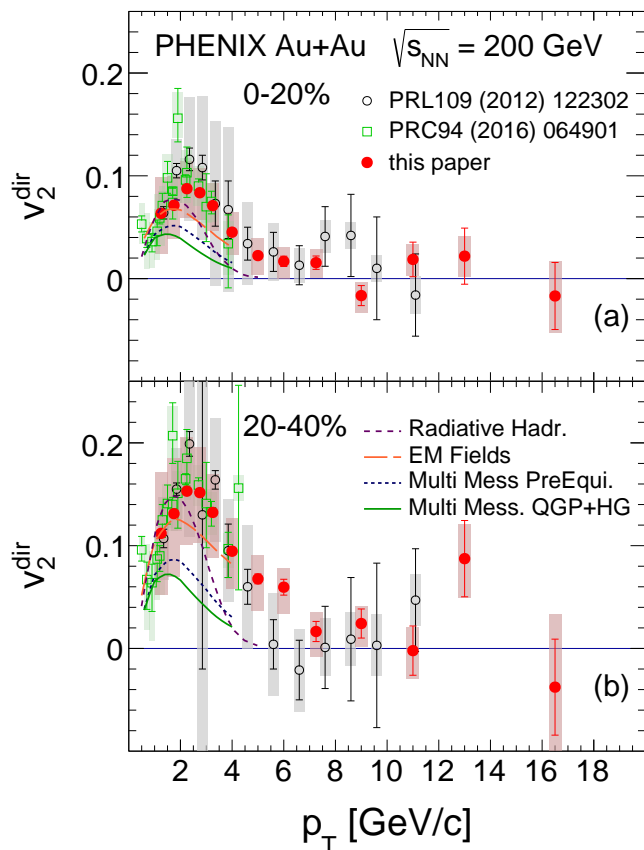


FIG. 9. Azimuthal anisotropy for 0%–20% (a) and 20%–40% (b). Again statistical errors are represented by lines, while systematic uncertainties are shown as shaded band. Some data points were moved slightly in p_T for clarity. The data is compared to previous measurements [22, 25] as well as to different theoretical models including pre-equilibrium contributions in the multimessenger model [9], modifications to such a scenario by the magnetic field present in the reaction volume [41], or radiative contributions at hadronization [37].

to extend anisotropies further in p_T , the modeled values for v_2^{dir} remain too low. One possible additional source could be a radiative contribution from the hadronization [37]. Adding this contribution to the emission from QGP and HG may achieve a more quantitative description of v_2^{dir} at low p_T [37], given in Fig. 9 as dashed line. However, the v_2^{dir} that the radiative hadronization adds is limited in its p_T reach to well below 4 GeV/c, whereas sizable v_2^{dir} values are experimentally observed at higher p_T .

Another conjectured source is the modified emission due to the electromagnetic fields created in the collision. Various aspects of possible modifications have been studied [38–41]. In a recent paper [41] it has been argued that the anisotropy of direct-photon emission may increase significantly, even when the fields are already substantially reduced in strength. Within the systematic uncertainties, considering this effect on top of the multimessenger approach with pre-equilibrium contribu-

tions leads to a promising agreement over the previously measured p_T range up to 4 GeV/c, as seen in the figure. In addition, this source may generate substantial v_2^{dir} even at higher p_T . It should be noted, however, that PHENIX also measured substantial third order Fourier component v_3 for direct photons [25], which is not discussed in [41], while earlier calculations of magnetic photon emission predicted vanishing v_3 [54]. The calculation of magnetic field effects [41] includes all sources from the multimessenger approach [9], but does not consider radiative hadronization, while the radiative hadronization calculation [37] ignores pre-equilibrium and magnetic effects. It would be interesting to see the results of a calculation with all those conjectured sources included.

VII. SUMMARY

To summarize, PHENIX presented the measurement of the azimuthal anisotropy of direct photons in Au+Au collisions at RHIC at $\sqrt{s_{NN}} = 200$ GeV, extending the range to p_T of 20 GeV/c. The dependence of the v_2^{dir} data on p_T and centrality may help set additional constraints and distinguish between proposed sources. For example, the contribution from radiative hadronization would be driven by the anisotropy and temperature of the source at hadronization. In contrast, emission modified by the electromagnetic fields would be sensitive to earlier times, higher temperatures, and the centrality dependence of the strength of the created fields.

Finally, at high $p_T > 10$ GeV/c, the direct-photon anisotropy is broadly consistent with zero for all centralities. Unlike π^0 or jets, prompt photons are not quenched, and thus should be unaffected by the collision geometry. The absence of an anisotropy supports the interpretation that direct photons in this p_T region are predominantly prompt photons from initial hard scatterings.

ACKNOWLEDGMENTS

We thank the staff of the Collider-Accelerator and Physics Departments at Brookhaven National Laboratory and the staff of the other PHENIX participating institutions for their vital contributions. We acknowledge support from the Office of Nuclear Physics in the Office of Science of the Department of Energy, the National Science Foundation, Abilene Christian University Research Council, Research Foundation of SUNY, and Dean of the College of Arts and Sciences, Vanderbilt University (U.S.A), Ministry of Education, Culture, Sports, Science, and Technology and the Japan Society for the Promotion of Science (Japan), Natural Science Foundation of China (People’s Republic of China), Croatian Science Foundation and Ministry of Science and Education (Croatia), Ministry of Education, Youth and Sports (Czech Republic), Centre National de la Recherche Scientifique, Commissariat à l’Énergie Atomique, and Institut

National de Physique Nucléaire et de Physique des Particules (France), J. Bolyai Research Scholarship, EFOP, HUN-REN ATOMKI, NKFIH, and OTKA (Hungary), Department of Atomic Energy and Department of Science and Technology (India), Israel Science Foundation (Israel), Basic Science Research and SRC(CENuM) Programs through NRF funded by the Ministry of Education and the Ministry of Science and ICT (Korea). Ministry of Education and Science, Russian Academy of Sciences,

Federal Agency of Atomic Energy (Russia), VR and Wallenberg Foundation (Sweden), University of Zambia, the Government of the Republic of Zambia (Zambia), the U.S. Civilian Research and Development Foundation for the Independent States of the Former Soviet Union, the Hungarian American Enterprise Scholarship Fund, the US-Hungarian Fulbright Foundation, and the US-Israel Binational Science Foundation.

-
- [1] I. Arsene *et al.* (BRAHMS Collaboration), Quark gluon plasma and color glass condensate at RHIC? The Perspective from the BRAHMS experiment, *Nucl. Phys. A* **757**, 1 (2005).
- [2] K. Adcox *et al.* (PHENIX Collaboration), Formation of dense partonic matter in relativistic nucleus-nucleus collisions at RHIC: Experimental evaluation by the PHENIX collaboration, *Nucl. Phys. A* **757**, 184 (2005).
- [3] B. B. Back *et al.* (PHOBOS Collaboration), The PHOBOS perspective on discoveries at RHIC, *Nucl. Phys. A* **757**, 28 (2005).
- [4] J. Adams *et al.* (STAR Collaboration), Experimental and theoretical challenges in the search for the quark gluon plasma: The STAR Collaboration's critical assessment of the evidence from RHIC collisions, *Nucl. Phys. A* **757**, 102 (2005).
- [5] E. V. Shuryak, Quark-gluon plasma and hadronic production of leptons, photons and psions, *Phys. Lett. B* **78**, 150 (1978).
- [6] P. Aurenche, A. Douiri, R. Baier, M. Fontannaz, and D. Schiff, Prompt Photon Production at Large p(T) in QCD Beyond the Leading Order, *Phys. Lett. B* **140**, 87 (1984).
- [7] J. F. Owens, Large Momentum Transfer Production of Direct Photons, Jets, and Particles, *Rev. Mod. Phys.* **59**, 465 (1987).
- [8] J.-F. Paquet, C. Shen, G. S. Denicol, M. Luzum, B. Schenke, S. Jeon, and C. Gale, Production of photons in relativistic heavy-ion collisions, *Phys. Rev. C* **93**, 044906 (2016).
- [9] C. Gale, J.-F. Paquet, B. Schenke, and C. Shen, Multimessenger heavy-ion collision physics, *Phys. Rev. C* **105**, 014909 (2022).
- [10] E. V. Shuryak and L. Xiong, Dilepton and photon production in the 'hot glue' scenario, *Phys. Rev. Lett.* **70**, 2241 (1993).
- [11] L. McLerran and B. Schenke, The Glasma, Photons and the Implications of Anisotropy, *Nucl. Phys. A* **929**, 71 (2014).
- [12] K. Tuchin, Photon decay in strong magnetic field in heavy-ion collisions, *Phys. Rev. C* **83**, 017901 (2011).
- [13] O. Linnyk, E. L. Bratkovskaya, and W. Cassing, Effective QCD and transport description of dilepton and photon production in heavy-ion collisions and elementary processes, *Prog. Part. Nucl. Phys.* **87**, 50 (2016).
- [14] C. Shen, U. W. Heinz, J.-F. Paquet, and C. Gale, Thermal photons as a quark-gluon plasma thermometer reexamined, *Phys. Rev. C* **89**, 044910 (2014).
- [15] H. van Hees, C. Gale, and R. Rapp, Thermal Photons and Collective Flow at the Relativistic Heavy-Ion Collider, *Phys. Rev. C* **84**, 054906 (2011).
- [16] K. Dusling and I. Zahed, Thermal photons from heavy ion collisions: A spectral function approach, *Phys. Rev. C* **82**, 054909 (2010).
- [17] S. Turbide, R. Rapp, and C. Gale, Hadronic production of thermal photons, *Phys. Rev. C* **69**, 014903 (2004).
- [18] M. Dion, J.-F. Paquet, B. Schenke, C. Young, S. Jeon, and C. Gale, Viscous photons in relativistic heavy ion collisions, *Phys. Rev. C* **84**, 064901 (2011).
- [19] T. Renk, Photon Emission from a Medium-Modified Shower Evolution, *Phys. Rev. C* **88**, 034902 (2013).
- [20] R. J. Fries, B. Muller, and D. K. Srivastava, High-energy photons from passage of jets through quark gluon plasma, *Phys. Rev. Lett.* **90**, 132301 (2003).
- [21] A. Adare *et al.* (PHENIX Collaboration), Enhanced production of direct photons in Au+Au collisions at $\sqrt{s_{NN}} = 200$ GeV and implications for the initial temperature, *Phys. Rev. Lett.* **104**, 132301 (2010).
- [22] A. Adare *et al.* (PHENIX Collaboration), Observation of direct-photon collective flow in $\sqrt{s_{NN}} = 200$ GeV Au+Au collisions, *Phys. Rev. Lett.* **109**, 122302 (2012).
- [23] S. Afanasiev *et al.* (PHENIX Collaboration), Measurement of Direct Photons in Au+Au Collisions at $\sqrt{s_{NN}} = 200$ GeV, *Phys. Rev. Lett.* **109**, 152302 (2012).
- [24] A. Adare *et al.* (PHENIX Collaboration), Centrality dependence of low-momentum direct-photon production in Au+Au collisions at $\sqrt{s_{NN}} = 200$ GeV, *Phys. Rev. C* **91**, 064904 (2015).
- [25] A. Adare *et al.* (PHENIX Collaboration), Azimuthally anisotropic emission of low-momentum direct photons in Au+Au collisions at $\sqrt{s_{NN}} = 200$ GeV, *Phys. Rev. C* **94**, 064901 (2016).
- [26] L. Adamczyk *et al.* (STAR Collaboration), Direct virtual photon production in Au+Au collisions at $\sqrt{s_{NN}} = 200$ GeV, *Phys. Lett. B* **770**, 451 (2017).
- [27] A. Adare *et al.* (PHENIX Collaboration), Beam Energy and Centrality Dependence of Direct-Photon Emission from Ultrarelativistic Heavy-Ion Collisions, *Phys. Rev. Lett.* **123**, 022301 (2019).
- [28] N. J. Abdulameer *et al.* (PHENIX Collaboration), Low-pT direct-photon production in Au+Au collisions at sNN=39 and 62.4 GeV, *Phys. Rev. C* **107**, 024914 (2023).
- [29] N. J. Abdulameer *et al.* (PHENIX Collaboration), Non-prompt direct-photon production in Au+Au collisions at sNN=200 GeV, *Phys. Rev. C* **109**, 044912 (2024).
- [30] J. Adam *et al.* (ALICE Collaboration), Direct photon production in Pb-Pb collisions at $\sqrt{s_{NN}} = 2.76$ TeV, *Phys. Lett. B* **754**, 235 (2016).

- [31] S. Acharya *et al.* (ALICE Collaboration), Direct photon elliptic flow in Pb-Pb collisions at $\sqrt{s_{NN}} = 2.76$ TeV, *Phys. Lett. B* **789**, 308 (2019).
- [32] G. David, Direct real photons in relativistic heavy ion collisions, *Rept. Prog. Phys.* **83**, 046301 (2020).
- [33] R. Chatterjee and P. Dasgupta, Probing Relativistic Heavy-Ion Collisions via Photon Anisotropic Flow Ratios. A Brief Review, *MDPI Physics* **6**, 674 (2024).
- [34] U. Heinz and R. Snellings, Collective flow and viscosity in relativistic heavy-ion collisions, *Ann. Rev. Nucl. Part. Sci.* **63**, 123 (2013).
- [35] R. Chatterjee and D. K. Srivastava, Elliptic flow of thermal photons and formation time of quark gluon plasma at RHIC, *Phys. Rev. C* **79**, 021901 (2009).
- [36] S. Campbell, Photon production from gluon-mediated quark-anti-quark annihilation at confinement, *Phys. Rev. C* **92**, 014907 (2015).
- [37] H. Fujii, K. Itakura, K. Miyachi, and C. Nonaka, Radiative hadronization: Photon emission at hadronization from quark-gluon plasma, *Phys. Rev. C* **106**, 034906 (2022).
- [38] G. Basar, D. E. Kharzeev, and V. Skokov, Conformal anomaly as a source of soft photons in heavy ion collisions, *Phys. Rev. Lett.* **109**, 202303 (2012).
- [39] B. Muller, S.-Y. Wu, and D.-L. Yang, Elliptic flow from thermal photons with magnetic field in holography, *Phys. Rev. D* **89**, 026013 (2014).
- [40] X. Wang, I. A. Shovkovy, L. Yu, and M. Huang, Ellipticity of photon emission from strongly magnetized hot QCD plasma, *Phys. Rev. D* **102**, 076010 (2020).
- [41] J. Sun and L. Yan, The Weak Magnetic Photon Emission from Quark-gluon Plasma, *Nucl. Phys. Rev.* **41**, 558 (2024).
- [42] S. Voloshin and Y. Zhang, Flow study in relativistic nuclear collisions by Fourier expansion of Azimuthal particle distributions, *Z. Phys. C* **70**, 665 (1996).
- [43] A. M. Poskanzer and S. A. Voloshin, Methods for analyzing anisotropic flow in relativistic nuclear collisions, *Phys. Rev. C* **58**, 1671 (1998).
- [44] M. Allen *et al.* (PHENIX Collaboration), PHENIX inner detectors, *Nucl. Instrum. Methods Phys. Res., Sec. A* **499**, 549 (2003).
- [45] L. Aphecetche *et al.* (PHENIX Collaboration), PHENIX calorimeter, *Nucl. Instrum. Methods Phys. Res., Sec. A* **499**, 521 (2003).
- [46] C. Aidala *et al.* (PHENIX Collaboration), The PHENIX Forward Silicon Vertex Detector, *Nucl. Instrum. Methods Phys. Res., Sec. A* **755**, 44 (2014).
- [47] J.-Y. Ollitrault, Anisotropy as a signature of transverse collective flow, *Phys. Rev. D* **46**, 229 (1992).
- [48] S. S. Adler *et al.* (PHENIX Collaboration), Identified charged particle spectra and yields in Au+Au collisions at $\sqrt{s_{NN}} = 200$ GeV, *Phys. Rev. C* **69**, 034909 (2004).
- [49] S. S. Adler *et al.* (PHENIX Collaboration), Suppressed π^0 production at large transverse momentum in central Au+ Au collisions at $\sqrt{s_{NN}} = 200$ GeV, *Phys. Rev. Lett.* **91**, 072301 (2003).
- [50] A. Adare *et al.* (PHENIX Collaboration), Suppression pattern of neutral pions at high transverse momentum in Au+Au collisions at $\sqrt{s_{NN}} = 200$ GeV and constraints on medium transport coefficients, *Phys. Rev. Lett.* **101**, 232301 (2008).
- [51] Y. Ren and A. Drees, Examination of the universal behavior of the η -to- π^0 ratio in heavy-ion collisions, *Phys. Rev. C* **104**, 054902 (2021).
- [52] A. Adare *et al.* (PHENIX Collaboration), Measurement of the higher-order anisotropic flow coefficients for identified hadrons in Au+Au collisions at $\sqrt{s_{NN}} = 200$ GeV, *Phys. Rev. C* **93**, 051902 (2016).
- [53] A. Adare *et al.* (PHENIX Collaboration), Measurements of elliptic and triangular flow in high-multiplicity $^3\text{He}+\text{Au}$ collisions at $\sqrt{s_{NN}} = 200$ GeV, *Phys. Rev. Lett.* **115**, 142301 (2015).
- [54] A. Bzdak and V. Skokov, Anisotropy of photon production: initial eccentricity or magnetic field, *Phys. Rev. Lett.* **110**, 192301 (2013).